High Precision Control for Parallel Twin-Drive Machine Tool System Based on Offline Parameter Identification Focusing on Differential Mode

Kota Fujimoto*a) Student Member, Hiroshi Fujimoto* Senior Member
Yoshihiro Isaoka** Member, Yuki Terada** Member

The size of the machine tool has been increasing to meet the demand for larger works, and recently the parallel twin-drive stage, which is actuated by two motors, is employed to drive the stage. On the other hand, the twin-drive stage has a problem of coupling force between the two motors, which degrades the tracking performance. In this paper, a novel offline parameter identification method focusing on the differential mode is proposed to improve the tracking performance of the twin-drive machine tool stage. The twin-drive stage is modeled as a two-inertia system for simplicity, and the inertia, viscosity, and coulomb coefficient are identified by the proposed method. The experiments are conducted to verify the proposed method, and it is confirmed that the tracking performance is improved by 49.7% with the identified parameters compared to the initial parameters.

Keywords: Machine tool, twin-drive stage, mode decoupling, sum/differential mode, parameter identification

1. Introduction

Machine tool, which is shown in Fig. 1, is a key equipment for manufacturing, and the demand for larger works has been increasing in recent years. To meet this demand, the size of the machine tool has been increasing, and the parallel twin-drive stage, which is actuated by two motors as shown in Fig. 2, is developed recently. Thanks to the twin-drive stage, the machine tool can drive the larger works with higer power, as well as more precise positioning with smaller motors. To the end, the numerous studies have been conducted to improve the tracking performance of the twin-drive stage.

In general, the feedforward (FF) control is implemented to improve the tracking performance[(1)–(3)]. However, only FF control is not sufficient to achieve the desired tracking performance due to the parameter error, modeling error, and disturbance. Therefore, the feedback (FB) control is also implemented to deal with these problems[(4)–(6)]. The compensation of the nonlinear forces such as nonlinear friction and backlash is also considered to improve the tracking performance[(7),(8)]. On the other hand, the significant problem of the twin-drive stage is rooted in the coupling force between the tandem motors, which degrades the tracking performance.

Coupling forces, which have a impact on the control performance, have been extensively addressed in several studies[(9)–(12)]. In Ref. (9), self-resonance cancellation (SRC) is proposed, which realizes the independent design of the resonance suppression and phase margin, although it does not consider the dual actuators. Ref. (10) proposed a decoupling control algorithm for multipule actuators, introducing the variable virtual actuator point to compensate the coupling force. In Ref. (11), the decoupling control method for parallel-link manupulators based on equivalent mass matrices is proposed, and Ref. (12) proposes a resonance suppression control method based on virtual resistance. These studies are beneficial for the high precision control of the twin-drive stage, though these methods are not directly applicable to the twin-drive stage in machine tool.

Although important contributions have been made to suppress the coupling force in the systems, the simple model di-

Figure 1: Example of machine tool with twin-drive stage.

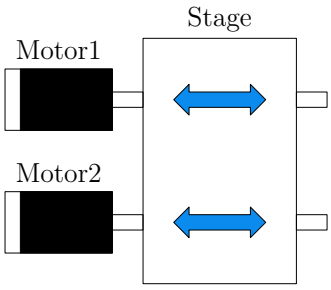

Figure 2: Image diagram of twin-drive stage.

a) Correspondence to: kota-fujimoto@ieee.org
* The University of Tokyo
5-1-5, Kashiwanoha, Kashiwa, Chiba 277-8561, Japan
** DMG MORI CO., LTD.
2-1, Sanjohonmachi, Nara , Nara, 630-8122, Japan

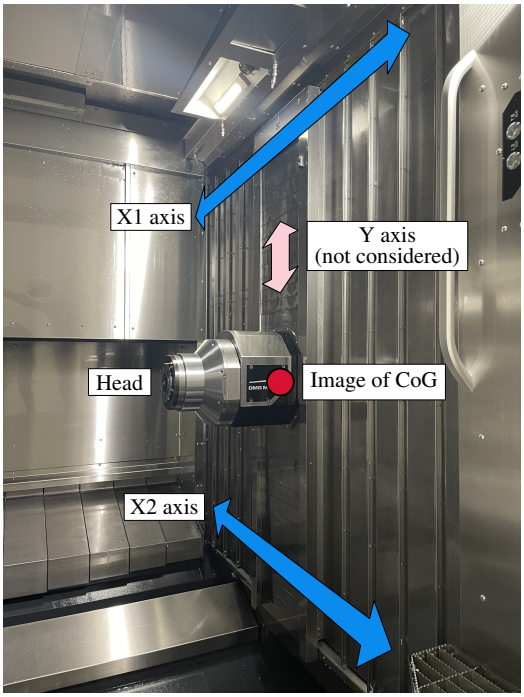

Figure 3: Experimental setup of twin-drive stage.

rectly applicable to the twin-drive machine tool stage is not taken into account in the previous studies. In one study, the model-based decoupling control method for the twin-drive machine tool stage with simple two-inertia model is proposed[13]. It is applicable to the actual machine tool; however, it does not consider the effect of the parameter error to improve the higher tracking performance. In another study, the model-based FF controller for twin-drive rotary tables is proposed, in which the parameter identification based on the genelic algorithm is conducted[14]. However, the proposed algorithm of the parameter identification is not siimple enough to be implemented in the actual machine tool. On the other hand, the developed approach in this study enables the offline parameter identification for the two-inertia model in simple procedures.

In this paper, a novel offline parameter identification method focusing on the differential mode is proposed to improve the tracking performance in twin-drive machine tool system. The twin-drive stage is modeled as a simple two-nertia system, and the offline parameter identification is conducted based on the differential mode of the two-inertia system. The propsed parameter identification method is verified by the experimental results with the twin-drive stage in the actual machine tool.

This paper is organized as follows. In section 2, the experimental setup is described, and the system model as well as the control system are introduced. In section 3, the proposed parameter identification method based on the differential mode is presented. In section 4, the experimental results both for parameter identification and tracking performance are shown. Finally, the paper is concluded and the future work is mentioned in section 5.

2. Problem formulation

2.1 Experimental setup

Fig. 3 shows the experimental setup of the twin-drive stage in an actual machine tool as shown in Fig. 1. The stage is mounted perpendicular to the ground and driven by two motors along the X1 and X2 axes. The head of the machine tool, where the cutting tools are attached, is mounted on the stage. The center of gravity (COG) of the stage is located around the head, and the image of the COG is shown is Fig. 3. Y axis also exists perpendicular to the X1 and X2 axes, but it is not considered in this paper.

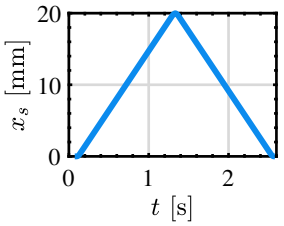

Figure 4: Position reference of sum mode for tracking performance evaluation.

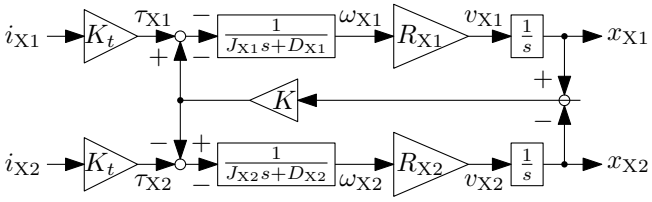

Figure 5: Block diagram of twin-drive stage as two-inertia system.

This experimental setup is utilized to investigate the tracking performance of the twin-drive stage for the reference trajectory as shown in Fig. 4. The stage go and return from 0 mm to 20 mm in 2.6 s. The RMSE of the error of the sum mode, which is detailed in section 2.3 as well as the differential mode, is evaluated in the final experiment as shown in section 4.2 compared to the conventional parameters.

2.2 Modeling of twin-drive stage as two-inertia system

In this paper, the twin-drive stage as shown in Fig. 3 is modeled as a two-inertia system for simplicity. The block diagram of the two-inertia system is shown in Fig. 5. i_{X1}, i_{X2}, τ_{X1}, τ_{X2} represent the motor currents of the X1 axis, X2 axis, and motor torques of the X1 axis, X2 axis, respectively. J_{X1}, D_{X1}, R_{X1}, J_{X2}, D_{X2}, R_{X2}, K, K_t represent the inertia, viscosity, ball screw rotation-to-translation ratio of the X1 axis motor, the inertia, viscosity coefficients, ball screw rotation-to-translation ratio of the X2 axis motor, the elasticity coefficient, and the motor torque coefficient, respectively. ω_{X1}, v_{X1}, x_{X1}, ω_{X2}, v_{X2}, x_{X2} represent the rotational speed of the X1 axis motor, stage velocity, stage position along X1 axis, rotational speed of the X2 axis motor, stage velocity, stage position along X2 axis, respectively. The equations of motion for this model are expressed as follows:

$$J'_{X1}\frac{d^2x_{X1}}{dt^2} + D'_{X1}\frac{dx_{X1}}{dt} + C'_{X1}\,\mathrm{sign}\,\frac{dx_{X1}}{dt} + K(x_{X1} - x_{X2}) = K_t i_{X1}, \tag{1a}$$

$$J'_{X2}\frac{d^2x_{X2}}{dt^2} + D'_{X2}\frac{dx_{X2}}{dt} + C'_{X2}\,\mathrm{sign}\,\frac{dx_{X2}}{dt} + K(x_{X2} - x_{X1}) = K_t i_{X2}, \tag{1b}$$

where

$$J'_{X1} = J_{X1}/R_{X1}, \quad D'_{X1} = D_{X1}/R_{X1}, \quad C'_{X1} = C_{X1}/R_{X1},$$
$$J'_{X2} = J_{X2}/R_{X2}, \quad D'_{X2} = D_{X2}/R_{X2}, \quad C'_{X2} = C_{X2}/R_{X2}.$$

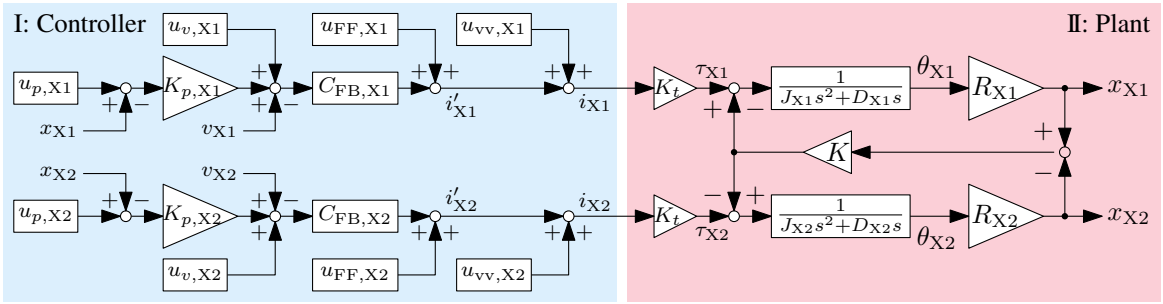

Figure 6: Block diagram of control system with mode decoupling.

C_{X1} and C_{X2} are the coulomb friction coefficients of the X1 axis and X2 axis, respectively. These coulomb friction is compensated based on the identified nominal values as $C'_{\mathrm{X1},n}$ and $C'_{\mathrm{X2},n}$. Therefore, the model considered in this paper is introduced as,

$$J'_{\mathrm{X1}}\frac{d^2x_{\mathrm{X1}}}{dt^2} + D'_{\mathrm{X1}}\frac{dx_{\mathrm{X1}}}{dt} + K\left(x_{\mathrm{X1}} - x_{\mathrm{X2}}\right) = K_t i_{\mathrm{X1}}, \quad (2a)$$

$$J'_{\mathrm{X2}}\frac{d^2x_{\mathrm{X2}}}{dt^2} + D'_{\mathrm{X2}}\frac{dx_{\mathrm{X2}}}{dt} + K\left(x_{\mathrm{X2}} - x_{\mathrm{X1}}\right) = K_t i_{\mathrm{X2}}. \quad (2b)$$

The initial nominal parameters of the two-inertia system are shown in Table. 1.

2.3 Mode decoupling with virtual viscosity In this part, the mode decoupling method of the two-inertia system from each axis mode as shown in (2) to sum/differential mode is detailed based on Ref. (13). Fig. 6 shows the block diagram of the control system implemented based on the previous study[15]. The mode decoupling is realized by adding the virtual viscosities $u_{\mathrm{vv,X1}}$ and $u_{\mathrm{vv,X2}}$ to the control input as shown in Fig. 6. In the figure, $u_{p,\mathrm{X1}}$, $u_{v,\mathrm{X1}}$, $u_{\mathrm{FF,X1}}$, $u_{p,\mathrm{X2}}$, $u_{v,\mathrm{X2}}$, $u_{\mathrm{FF,X2}}$ are the reference value of position, reference value of velocity, and feedforward input in the X1 axis and X2 axis, respectively. All the reference values are generated based on the algorithm of perfect tracking control detailed in Ref. (1), with which the zero-error tracking is accomplished at the sampling points of the feedback signal. $K_{p,\mathrm{X1}}$, $K_{p,\mathrm{X2}}$ are the proportional gain of the position controller in the X1 axis and X2 axis, respectively. $C_{\mathrm{FB,X1}}$, $C_{\mathrm{FB,X2}}$ are the velocity controller implemented as a PI controller in the X1 axis and X2 axis, respectively. i'_{X1} and i'_{X2} are the current in the X1 axis without virtual viscosity, and current in the X2 axis without virtual viscosity, respectively.

Considering only the control inputs $i'_{t,\mathrm{X1}}$, $i'_{t,\mathrm{X2}}$, without the virtual viscosity, the equations of motion on the two-inertia system based on Eq. (2) are given as,

$$J'_{\mathrm{X1}}\frac{d^2x_{\mathrm{X1}}}{dt^2} + D'_{\mathrm{X1}}\frac{dx_{\mathrm{X1}}}{dt} + K\left(x_{\mathrm{X1}} - x_{\mathrm{X2}}\right) = K_t i'_{\mathrm{X1}}, \quad (3a)$$

$$J'_{\mathrm{X2}}\frac{d^2x_{\mathrm{X2}}}{dt^2} + D'_{\mathrm{X2}}\frac{dx_{\mathrm{X2}}}{dt} + K\left(x_{\mathrm{X2}} - x_{\mathrm{X1}}\right) = K_t i'_{\mathrm{X2}}. \quad (3b)$$

We consider adding control inputs as torques, such as $K_t i'_{v,\mathrm{X1}}$ and $K_t i'_{v,\mathrm{X2}}$, to the right-hand side of Eq. (3). Assuming these control inputs are linear with respect to the stage velocity of each axis, and denoting the coefficients as a_{X1}, a_{X2}, we can express $K_t i'_{v,\mathrm{X1}} = a_{\mathrm{X1}}\frac{dx_{\mathrm{X1}}}{dt}$ and $K_t i'_{v,\mathrm{X2}} = a_{\mathrm{X2}}\frac{dx_{\mathrm{X2}}}{dt}$. Then, Eq. (3) becomes,

Table 1: Initial nominal normalized parameter of two-inertia system in this paper.

Parameter	Value
Motor Inertia along X1 axis $J'_{\mathrm{X1,n0}}$	26.5 mkgm^2
Motor Viscosity along X1 axis $D'_{\mathrm{X1,n0}}$	14.8 mNms/rad
Motor Inertia along X2 axis $J'_{\mathrm{X2,n0}}$	39.5 mkgm^2
Motor Viscosity along X2 axis $D'_{\mathrm{X2,n0}}$	15.1 mNms/rad
Torsional Rigidity K	8700 Nm/rad
Motor Torque Coefficient K_t	1.95 Nm/A

$$J'_{\mathrm{X1}}\frac{d^2x_{\mathrm{X1}}}{dt^2} + \left(D'_{\mathrm{X1}} - a_{\mathrm{X1}}\right)\frac{dx_{\mathrm{X1}}}{dt} + K\left(x_{\mathrm{X1}} - x_{\mathrm{X2}}\right) = K_t i'_{t,\mathrm{X1}}, \quad (4a)$$

$$J'_{\mathrm{X2}}\frac{d^2x_{\mathrm{X2}}}{dt^2} + \left(D'_{\mathrm{X2}} - a_{\mathrm{X1}}\right)\frac{dx_{\mathrm{X2}}}{dt} + K\left(x_{\mathrm{X2}} - x_{\mathrm{X1}}\right) = K_t i'_{t,\mathrm{X2}}. \quad (4b)$$

To convert Eq. (4) into the COG coordinate system, the below equations should be established:

$$\frac{D'_{\mathrm{X1}} - a_{\mathrm{X1}}}{J'_{\mathrm{X1}}} = \frac{D'_{\mathrm{X2}} - a_{\mathrm{X1}}}{J'_{\mathrm{X2}}} (= b). \quad (5)$$

In this paper, The condition $a_{\mathrm{X1}} = 0$ is assumed. Then,

$$a_{\mathrm{X1}} = D'_{\mathrm{X2}} - \frac{J'_{\mathrm{X2}}}{J'_{\mathrm{X1}}}D'_{\mathrm{X1}}. \quad (6)$$

Under Eqs. (5) and (6), transforming Eq. (4) results in,

$$J'_{\mathrm{X1}}\frac{d^2x_{\mathrm{X1}}}{dt^2} + bJ'_{\mathrm{X1}}\frac{dx_{\mathrm{X1}}}{dt} + K\left(x_{\mathrm{X1}} - x_{\mathrm{X2}}\right) = K_t i'_{\mathrm{X1}}, \quad (7a)$$

$$J'_{\mathrm{X2}}\frac{d^2x_{\mathrm{X2}}}{dt^2} + bJ'_{\mathrm{X2}}\frac{dx_{\mathrm{X2}}}{dt} + K\left(x_{\mathrm{X2}} - x_{\mathrm{X1}}\right) = K_t i'_{\mathrm{X2}}. \quad (7b)$$

Regarding Eq. (7), if we sum up both sides of Eqs. (7a) and (7b) and divide by $J'_{\mathrm{X1}} + J'_{\mathrm{X2}}$, or divide both sides of Eqs. (7a) and (7b) by J'_{X1} and J'_{X2} respectively before subtracting them, the equations of motion expressed in sum and differential modes are derived as,

$$\frac{d^2x_s}{dt^2} + b\frac{dx_s}{dt} = K_t i_s, \quad (8a)$$

$$\frac{d^2x_d}{dt^2} + b\frac{dx_d}{dt} + \left(\frac{K}{J'_{\mathrm{X1}}} + \frac{K}{J'_{\mathrm{X2}}}\right)x_d = K_t i_d. \quad (8b)$$

where x_s and x_d are the sum mode and differential mode of

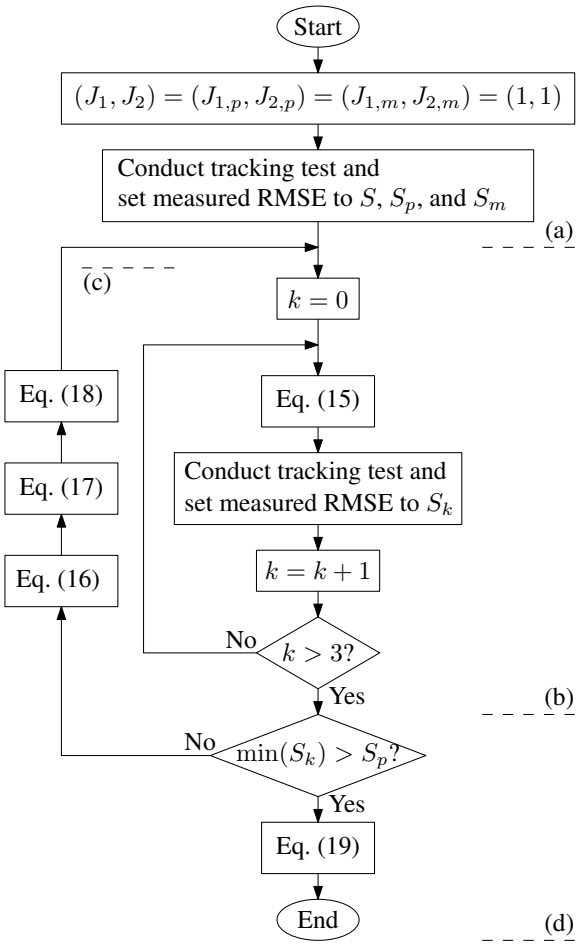

Figure 7: Flowchart of parameter identification algorithm regarding inertia as example.

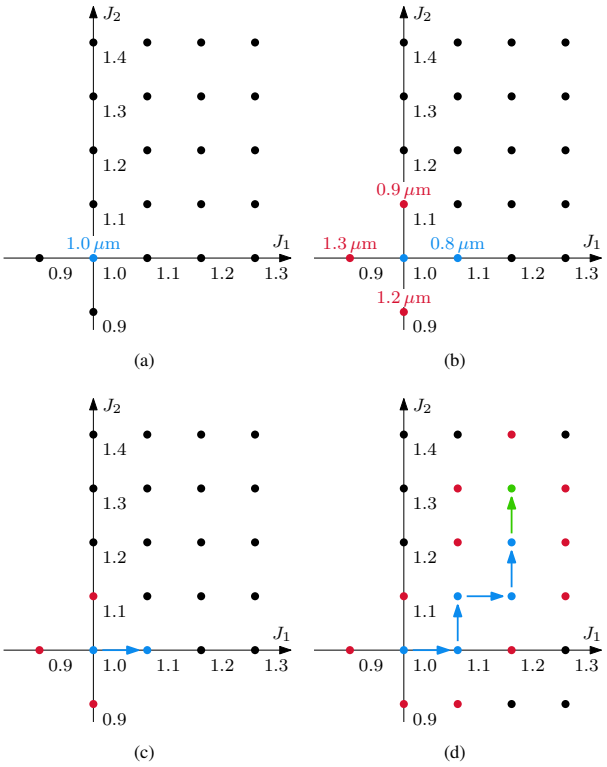

Figure 8: Diagrams of parameter identification algorithm regarding inertia as example. (a) Calculate RMSE at current (start) point. (b) Calculate RMSE around current point. (c) Update position of current point. (d) Update parameters for optimal point.

the twin-drive stage, respectively. Here, i_{sum} and i_d are expressed as,

$$\begin{bmatrix} x_s \\ x_d \end{bmatrix} = \begin{bmatrix} \frac{J'_{\mathrm{X1}}}{J'_{\mathrm{X1}}+J'_{\mathrm{X2}}} & \frac{J'_{\mathrm{X2}}}{J'_{\mathrm{X1}}+J'_{\mathrm{X2}}} \\ 1 & -1 \end{bmatrix} \begin{bmatrix} x_{\mathrm{X1}} \\ x_{\mathrm{X2}} \end{bmatrix} = M_{12,\mathrm{sd}} \begin{bmatrix} x_{\mathrm{X1}} \\ x_{\mathrm{X2}} \end{bmatrix}, \tag{9a}$$

$$\begin{bmatrix} i'_{t,\mathrm{X1}} \\ i'_{t,\mathrm{X2}} \end{bmatrix} = \begin{bmatrix} J'_{\mathrm{X1}} & \frac{J'_{\mathrm{X1}}J'_{\mathrm{X2}}}{J'_{\mathrm{X1}}+J'_{\mathrm{X2}}} \\ J'_{\mathrm{X2}} & -\frac{J'_{\mathrm{X1}}J'_{\mathrm{X2}}}{J'_{\mathrm{X1}}+J'_{\mathrm{X2}}} \end{bmatrix} \begin{bmatrix} i_s \\ i_d \end{bmatrix} = M_{\mathrm{sd},12} \begin{bmatrix} i_s \\ i_d \end{bmatrix}. \tag{9b}$$

Hence, the coupling system represented by Eq. (3) can be converted into decoupling modes as shown in Eq. (8) by adding the virtual viscosity.

3. Proposed parameter identification method based on differential mode

In this section, the proposed parameter identification method based on the differential mode is described. First, the model derived in the previous section is analyzed to show how the parameters are identified regarding the differential mode. Then, the parameter identification algorithm is presented for actual machine tools.

3.1 Model analysis for parameter identification focusing on differential mode In this part, the model in Eq. (2) is analyzed for parameter identification. From Eq. (2a), the differential mode is shown as,

$$x_{\mathrm{X1}} - x_{\mathrm{X2}} = -\frac{1}{K}\left(J'_{\mathrm{X1}}\frac{d^2x_{\mathrm{X1}}}{dt^2} + D'_{\mathrm{X1}}\frac{dx_{\mathrm{X1}}}{dt} - K_t i_{\mathrm{X1}}\right). \tag{10}$$

As the same way, the differential mode ragarding Eq. (2b) is expressed as,

$$x_{\mathrm{X1}} - x_{\mathrm{X2}} = \frac{1}{K}\left(J'_{\mathrm{X2}}\frac{d^2x_{\mathrm{X2}}}{dt^2} + D'_{\mathrm{X2}}\frac{dx_{\mathrm{X2}}}{dt} - K_t i_{\mathrm{X2}}\right). \tag{11}$$

For the proposed parameter identification, the perfect tracking control algorithm based on Ref. (1) is employed referring to the model in Eq. (2) as,

$$J'_{\mathrm{X1},n}\frac{d^2x_{\mathrm{X1}}}{dt^2} + D'_{\mathrm{X1},n}\frac{dx_{\mathrm{X1}}}{dt} = K_{t,n} i_{\mathrm{X1}}, \tag{12a}$$

$$J'_{\mathrm{X1},n}\frac{d^2x_{\mathrm{X2}}}{dt^2} + D'_{\mathrm{X2},n}\frac{dx_{\mathrm{X2}}}{dt} = K_{t,n} i_{\mathrm{X2}}, \tag{12b}$$

where the subscript n represents the nominal model parameter. Based on (12), Eqs. (10) and (11) are transformed as,

$$\begin{aligned} x_{\mathrm{X1}} - x_{\mathrm{X2}} &= -\frac{1}{K}\left(J'_{\mathrm{X1}}\frac{d^2x_{\mathrm{X1}}}{dt^2} + D'_{\mathrm{X1}}\frac{dx_{\mathrm{X1}}}{dt} - J'_{\mathrm{X1},n}\frac{d^2x_{\mathrm{X1}}}{dt^2} + D'_{\mathrm{X1},n}\frac{dx_{\mathrm{X1}}}{dt}\right), \\ &= -\frac{1}{K}\left(\Delta J'_{\mathrm{X1}}\frac{d^2x_{\mathrm{X1}}}{dt^2} + \Delta D'_{\mathrm{X1}}\frac{dx_{\mathrm{X1}}}{dt}\right), \end{aligned} \tag{13a}$$

$$\begin{aligned} x_{\mathrm{X1}} - x_{\mathrm{X2}} &= \frac{1}{K}\left(J'_{\mathrm{X2}}\frac{d^2x_{\mathrm{X2}}}{dt^2} + D'_{\mathrm{X2}}\frac{dx_{\mathrm{X2}}}{dt} - J'_{\mathrm{X2},n}\frac{d^2x_{\mathrm{X2}}}{dt^2} + D'_{\mathrm{X2},n}\frac{dx_{\mathrm{X2}}}{dt}\right), \\ &= \frac{1}{K}\left(\Delta J'_{\mathrm{X2}}\frac{d^2x_{\mathrm{X2}}}{dt^2} + \Delta D'_{\mathrm{X2}}\frac{dx_{\mathrm{X2}}}{dt}\right). \end{aligned} \tag{13b}$$

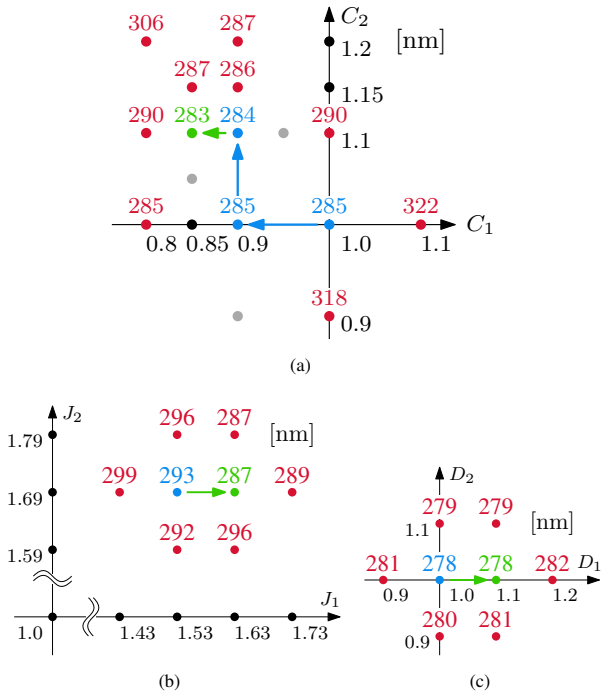

Figure 9: Experimental results of parameter identification based on differential mode. (a) Coulomb friction. (b) Inertia. (c) Viscosity.

From (13), it can be said that the parameter error of inertia and viscotiy becomes almost zero if $x_{X1} - x_{X2}$ is sufficiently smaller than the absolute value of $1/K$.

3.2 Parameter identification algorithm for twin-drive machine tool Fig. 7 shows the flowchart of the parameter identification algorithm. Fig. 7 describes the identification algorithm for inertia as an example, though the same algorithm is also applied to identify viscosity and coulomb coefficient. In the proposed algorithm, normalized inertia J_1 and J_2 are defined as,

$$J_1 = \frac{J'_{X1,n}}{J'_{X1,n0}}, \quad J_2 = \frac{J'_{X2,n}}{J'_{X2,n0}}, \tag{14}$$

where $J'_{X1,n0}$ and $J'_{X2,n0}$ are the initial values of the nominal model parameter. The normalized viscosity D_1 and D_2, and the normalized coulomb coefficient C_1 and C_2 are also defined in the same way. S is utilized to measure the root mean square error (RMSE) of the differential mode error in each tracking test. Subscripts p and m represent the previous value and the value for the memory, respectively. ΔJ_1 and ΔJ_2 are the increment value for the normalized inertia. k is the iteration number of the parameter identification algorithm.

The diagrams of the parameter identification algorithm are shown in Fig. 8. The simbols (a)–(d) in Fig. 8 correspond to the steps (a)–(d) in Fig. 7. The detailed steps of the algorithm are as follows: First, the tracking test for the reference trajectory as shown in Fig. 4 with the initial normalized parameter is conducted. Then, the RMSE of differential mode error is calculated and memorized to S, S_p, and S_m. This step corresponds to Fig. 8(a). In Fig. 8(a), the RMSE is written above the blue dot as 1.0 µm, for example.

Second, the nominal normalized parameters are changed around the current point for four directions as shown in Fig. 8(b). The parameters are changed with the iteration number k as,

$$(J_1, J_2) = \left(J_{1,p} + \Delta J_1 \cos\frac{\pi}{2}k, J_{2,p} + \Delta J_2 \sin\frac{\pi}{2}k\right). \tag{15}$$

Then, the tracking test is conducted, and the RMSE of the differential mode error is calculated at each point. The iteration continues until $k > 3$ as shown in Fig. 7. All the calculated RMSE are compared with the RMSE at the current position, and the direction to minimize the RMSE is examined as shown in Fig. 8(b). In Fig. 8(b), the dot is colored with blue if the RMSE is smaller than the current point, and with red if the RMSE is larger than the current point. In this example, the current point is updated for the direction to minimize the RMSE as shown in Fig. 8(c).

After deciding the update direction, the minumum value of S_k and its iteration number k is memorized for the next iteration as,

$$S_p = \min(S_k), \quad k = \operatorname{argmin}(S_k). \tag{16}$$

Then, the normalized parameters are updated based on the iteration number just memorized as,

$$(J_{1,m}, J_{2,m}) = \left(J_{1,m} + \Delta J_1 \cos\frac{\pi}{2}k, J_{2,m} + \Delta J_2 \sin\frac{\pi}{2}k\right). \tag{17}$$

Finally, $J_{1,p}$ and $J_{2,p}$ are also updated as,

$$(J_{1,p}, J_{2,p}) = (J_{1,m}, J_{2,m}). \tag{18}$$

This procedure is repeated until the RMSE converges to the minimum value as shown in Fig. 8(d). In Fig. 8(d), the optimal point is colored with green. To the end, the identified parameters are obtained as,

$$(J_1, J_2) = (J_{1,m}, J_{2,m}). \tag{19}$$

This is just an example of the parameter identification algorithm for inertia, and the same algorithm is also applied to identify viscosity and coulomb coefficient.

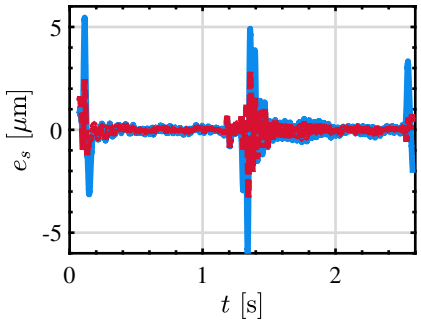

Figure 10: Sum mode tracking error. Tracking error with initial parameters (—). Tracking error with identified parameters (—).

Table 2: Tracking results betwen initial and identified parameters for ten trials.

	RMSE	Standard deviation
Initial parameters	0.860 µm (0.0 %)	7.62 nm
Identified parameters	0.433 µm (−49.7 %)	10.2 nm

4. Experiment

In this section, the experimental verification of the proposed method is detailed. First, the results of the parameter identification are described. Then, the tracking performance of the twin-drive stage is evaluated based on the identified parameters, while comparing with the initial parameters.

4.1 Parameter identification based on differential mode Fig. 9 shows the experimental results of the parameter identification based on the differential mode. The RMSE of the differential mode is written above each dot as the results of each trial. Regarding the value order of the RMSE, it is confirmed that the nominal parameters can be sufficiently identified by the proposed method because the RMSE order of the differential mode (10^{-7}) is much smaller than the order of $1/K$ (10^{-4}).

At first, the normalized coulomb coefficient C_1 and C_2 are identified, and the results are shown in Fig. 9(a). The normalized coulomb coefficients are updated from $(C_1, C_2) = (1.0, 1.0)$ to $(C_1, C_2) = (0.85, 1.1)$. The increment of the coulomb coefficient ΔC_1 and ΔC_2 are firstly set as 0.1, and the increment is updated to 0.05 at the final transition. The grey points in Fig. 9(a) represent some missing results. These results are utilized to suppress the effect of the coulomb friction in Eq. (1), and establish Eq. (2).

Then, the normalized inertia J_1 and J_2 are identified with the identified normalized coulomb coefficients, and the results are shown in Fig. 9(b). The start point of the inertia identification is set as $(J_1, J_2) = (1.53, 1.69)$ in this paper, and the normalized inertia are updated from $(J_1, J_2) = (1.53, 1.69)$ to $(J_1, J_2) = (1.63, 1.69)$. The increment of the inertia ΔJ_1 and ΔJ_2 are set as 0.1.

Finally, the normalized viscosity D_1 and D_2 are identified with the identified normalized coulomb coefficients and normalized inertia, and the results are shown in Fig. 9(c). The normalized viscosity are updated from $(D_1, D_2) = (1.0, 1.0)$ to $(D_1, D_2) = (1.1, 1.0)$. The increment of the viscosity ΔD_1 and ΔD_2 are set as 0.1. These identified values are verified in the next section to conduct the tracking performance evaluation.

4.2 Tracking performance evaluation between initial and identified parameters The tracking performance evaluation is conducted to compare the performance between the initial parameters and the identified parameters. Fig. 10 shows the sum mode tracking error of the twin-drive stage. It is confirmed that the tracking peformance is improved by the identified parameters, especially for the transient response. Table. 2 shows the experimental result analysis for the ten times tracking experiments. The RMSE of the sum mode tracking error is reduced from 0.860 μm to 0.433 μm, which is a reduction of 49.7 %. It is also confirmed that the standard deviation of the tracking error is sufficiently small to mention the enough repeatability of the tracking performance.

5. Conclusion

In this paper, the parameter identification method based on the differential mode was proposed for the twin-drive stage in machine tool. The twin-drive stage was modeled as a two-inertia system, and the model parameters such as inertia, viscosity, and coulomb coefficient were identified based on the differential mode combined with the model-based feedforward control algorithm. The experimental results showed that the tracking performance was improved by 49.7 % with the identified parameters compared to the initial parameters. In this paper, the parameter was determined in the narrow range on the twin-drive stage as offline identification. The proposed method will be expanded to the online identification in the future work.

References

(1) H. Fujimoto, Y. Hori, and A. Kawamura, "Perfect tracking control based on multirate feedforward control with generalized sampling periods," *IEEE Transactions on Industrial Electronics*, vol. 48, no. 3, pp. 636–644, 2001.

(2) M. Mae, W. Ohnishi, and H. Fujimoto, "MIMO multirate feedforward controller design with selection of input multiplicities and intersample behavior analysis," *Mechatronics*, vol. 71, p. 102442, 2020.

(3) M. Poot, J. Portegies, N. Mooren, M. van Haren, M. van Meer, and T. Oomen, "Gaussian processes for advanced motion control," *IEEJ Journal of Industry Applications*, vol. 11, no. 3, pp. 396–407, 2022.

(4) T. Kai, H. Sekiguchi, and H. Ikeda, "Control structure with dual acceleration feedback for positioning machine with Semi-Closed servo system," *IEEJ Journal of Industry Applications*, vol. 11, no. 2, pp. 351–358, 2022.

(5) S. Yabui and T. Inoue, "Development of optimal controller design method to compensate for vibrations caused by unbalanced force in rotor system based on nyquist diagram," *Journal of Vibration and Control*, vol. 25, no. 4, pp. 793–805, 2019.

(6) S. Yamada, K. Inukai, H. Fujimoto, K. Omata, Y. Takeda, and S. Makinouchi, "Proposal of self resonance cancellation control without using drive-side information," in *IEEE 41st Annual Conference of the IEEE Industrial Electronics Society (IECON)*, 2015.

(7) T. Hayashi, H. Fujimoto, Y. Isaoka, and Y. Terada, "Projection-based iterative learning control for ball-screw-driven stage with consideration of rolling friction compensation," *IEEJ Transactions on Industry Applications*, vol. 9, no. 2, pp. 132–139, 2020.

(8) J. Padron, Y. Yokokura, K. Ohishi, T. Miyazaki, and Y. Kawai, "Evaluating the equivalence between nonlinear friction and backlash in Two-Inertia systems," in *IEEE 17th International Conference on Advanced Motion Control (AMC)*, pp. 335–340, 2022.

(9) K. Sakata, H. Asaumi, K. Hirachi, K. Saiki, and H. Fujimoto, "Self resonance cancellation techniques for a Two-Mass system and its application to a Large-Scale stage," *IEEJ Journal of Industry Applications*, vol. 3, no. 6, pp. 455–462, 2014.

(10) W. Ohnishi, H. Fujimoto, K. Sakata, K. Suzuki, and K. Saiki, "Decoupling control method for high-precision stages using multiple actuators considering the misalignment among the actuation point, center of gravity, and center of rotation," *IEEJ Journal of Industry Applications*, vol. 5, no. 2, pp. 141–147, 2016.

(11) K. Shimamoto and T. Murakami, "Force sensorless hybrid Position/Force control with equivalent mass matrices switching for decoupled rubbing motion," *IEEJ Journal of Industry Applications*, vol. 12, no. 2, pp. 107–116, 2023.

(12) K. Natori, A. Ishikawa, and Y. Sato, "A study on resonance suppression control based on virtual resistance concept for parallel inverters in islanded microgrid," in *2020 9th International Power Electronics and Motion Control Conference (IPEMC2020-ECCE Asia)*, pp. 2018–2024, 2020.

(13) K. Fujimoto, H. Fujimoto, Y. Isaoka, and Y. Terada, "High precision control for twin-drive system of machine tool based on mode decoupling with virtual viscosity: Basic study on two-inertia system," in *IEE-Japan Technical Meeting on Mechatronics Control (PSS)*, 2023.

(14) K. Ito, W. Maebashi, J. Ikeda, and M. Iwasaki, "Fast and Precise Positioning of Rotary Table Systems by Feedforward Disturbance Compensation Considering Interference Force," in *IECON 2011 - 37th Annual Conference of the IEEE Industrial Electronics Society*, pp. 3382–3387, 2011.

(15) K. Fujimoto, H. Fujimoto, Y. Isaoka, and Y. Terada, "High precision control for twin-drive system based on mode decoupling with virtual viscosity: Equivalent controller transform for machine tool," in *2024 18th International Conference on Advanced Motion Control (AMC)*, 2024.